IEEE Access
Multidisciplinary ⋮ Rapid Review ⋮ Open Access Journal

Received August 26, 2021, accepted September 17, 2021, date of publication September 20, 2021,
date of current version September 27, 2021.

Digital Object Identifier 10.1109/ACCESS.2021.3114182

A Fractional-Order Transitional Butterworth-Butterworth Filter and Its Experimental Validation

SHIBENDU MAHATA[1], NORBERT HERENCSAR[2], (Senior Member, IEEE), DAVID KUBANEK[2], RAJIB KAR[3], (Senior Member, IEEE), DURBADAL MANDAL[3], (Member, IEEE), AND İ. CEM GÖKNAR[4], (Life Fellow, IEEE)

[1]Department of Instrumentation and Electronics Engineering, Dr. B. C. Roy Engineering College, Durgapur, West Bengal 713206, India
[2]Department of Telecommunications, Faculty of Electrical Engineering and Communication, Brno University of Technology, 61600 Brno, Czechia
[3]Department of Electronics and Communication Engineering, National Institute of Technology Durgapur, Durgapur 713209, India
[4]Department of Electrical and Electronics Engineering, Işik University, 34980 Şile/Istanbul, Turkey

Corresponding author: Norbert Herencsar (herencsn@ieee.org)

This work was supported by Czech Science Foundation under Project 19-24585S.

ABSTRACT This paper introduces the generalization of the classical Transitional Butterworth-Butterworth Filter (TBBF) to the Fractional-Order (FO) domain. Stable rational approximants of the FO-TBBF are optimally realized. Several design examples demonstrate the robustness and modeling efficacy of the proposed method. Practical circuit implementation using the current feedback operational amplifier employed as an active element is presented. Experimental results endorse good agreement ($R^2 = 0.999968$) with the theoretical magnitude-frequency characteristic.

INDEX TERMS Analog filter approximation, analog signal processing, current feedback operational amplifier, fractional-order filter, transitional filter.

I. INTRODUCTION

The modeling techniques and realization of classical (integer-order) analog filters are well-established. To further improve the performance of such filters (e.g., reduction in pass-band error, sharper transition-band characteristic), the use of graphical methods [1] and optimal procedures [2]–[4] have been adopted.

Recently, the theoretical concept of fractional calculus, which deals with the generalization of the classical definitions of differentiation and integration, has been applied to achieve a more precise attenuation behavior of analog filters [5]. This is possible due to the generalization of the classical Laplacian operator s to the Fractional-Order (FO) form s^α, where $\alpha \in (0, 1)$, which causes additional degrees of freedom in system modeling. The impedance function containing the s^α operator may be realized using fractance devices or Constant Phase Elements (CPE) [6]. Due to the commercial unavailability of these devices, CPE emulators in the integrated form [7] or discrete-components-based [8] have been reported. The s^α operator forms the basic building block of the FO transfer functions, which can lead to generalizations of classical Butterworth filter [9], oscillators [10], and resonators [11]. Both active and passive elements have been employed to realize the FO impedances [12], [13]. Another popular method is to approximate the FO system using the integer-order transfer function [14]. The exact dynamics of a FO system can be theoretically achieved by a system of infinite integer order. For practical purposes, the characteristics of the FO filter need to be approximated using a finite-order rational approximant. An integer-order model of lower-order is desirable since it results in smaller hardware overhead. The rational approximation of s^α may be achieved using frequency-domain-based curve fitting [15], a weighted sum of first-order optimal high-pass filter sections [16], etc.

Transitional filters merge the frequency responses of various classical filters (e.g., Butterworth, Chebyshev, Bessel, Legendre, Thomson) to attain conciliation between the amplitude and group delay characteristics [17]. Transitional filters may be designed by combining different filter poles using the arithmetic or geometric interpolation, as exemplified by the transitional Legendre-Thomson filter [18], and the transitional ultraspherical-ultraspherical filter [19]. An alternative

The associate editor coordinating the review of this manuscript and approving it for publication was Qi Zhou.

TABLE 1. Comparison with the existing FOBF and TBBF design techniques.

Reference	Design	Advantages	Limitations
[9]	FOBF	Analytically derived expressions for model coefficients	Cannot model TBBF characteristics; Non-optimal technique
[20]	TBBF	Based on interpolation of classical Butterworth filters	Cannot model fractional-step characteristics of TBBFs
[21], [22]	FOBF	Circuit realization does not require CPE or CPE-emulators	Cannot model TBBF characteristics; Stability conditions based on both bound and nonlinear inequality constraints
Present Work	FO-TBBF	Optimal TBBF models exhibiting fractional-step behavior; Guaranteed stability using lower bound constraints only	Iterative method

design technique involves combining the classical filter polynomials [20]. The magnitude squared function of the classical Transitional Butterworth-Butterworth Filter (TBBF) is given by (1) [20]:

$$|H(j\omega)|^2 = \frac{1}{1+\varepsilon^2(\omega^{2n}+\omega^{2k})}, \tag{1}$$

where n and k are integers, $0 \leq k \leq n$; ε is the ripple constant; and ω is the angular frequency in radians per second (rad/s). For $n = k$, and rewriting the ripple constant as $\varepsilon/\sqrt{2}$, the magnitude characteristics of the n^{th} order Butterworth filter can be also obtained from (1). The response of the TBBF comprises the arithmetic interpolation between two classical Butterworth filters. It may be inferred from (1) that for $n > k$, the dominating responses in the passband and stopband regions are due to the k^{th} order and the n^{th} order Butterworth filters, respectively. Hence, the passband and stopband responses of the TBBF can be nearly independently adjusted.

Optimization techniques were employed to approximate the characteristics of the FO Butterworth Filter (FOBF) [21], [22]. However, to the best of the authors' knowledge, no literature exists on the FO modeling of TBBFs. This paper introduces the definition of FO-TBBF characteristic by removing the restrictions of integer values for n and k imposed in (1). Optimal rational approximations are proposed, which can meet the theoretical magnitude-frequency behavior of the FO-TBBF. Design stability is ensured by representing the denominator polynomial of the proposed model as a cascade of first-order and second-order terms comprising positive coefficients. Thus, inequality constraints are avoided to meet the s-domain stability criteria. Table 1 compares the advantages and limitations of the proposed method with those of the FOBF [9], [21], [22], and TBBF [20] design techniques. Several design cases are considered to evaluate the performance of the proposed technique. Current Feedback Operational Amplifier (CFOA) [23] based hardware circuit implementation of the proposed FO-TBBF approximant is demonstrated. Simulation and experimental results confirm excellent agreement with the ideal magnitude characteristics.

In the rest of the paper, the proposed technique is presented in Section II. MATLAB simulations are carried out to highlight the modeling efficiency in Section III. Section IV presents the circuit implementation and measurement results, while conclusions are drawn in Section V.

II. DESIGN METHODOLOGY

A. DEFINITION

The theoretical squared-magnitude function for the FO-TBBF is proposed according to (2):

$$|B(j\omega)|^2 = \frac{1}{1+\varepsilon^2[\omega^{2(n_1+\alpha)}+\omega^{2(n_2+\beta)}]}, \tag{2}$$

where n_1 and n_2 are integer numbers, $\alpha, \beta \in [0, 1]$, and $(n_1+\alpha) \geq (n_2+\beta)$. For $\alpha = \beta = 0$ and 1, the TBBF can be treated as a special case of the FO-TBBF. Note that (2) may yield the definition of a FOBF when $(n_1+\alpha) = (n_2+\beta)$. The proposed definition also allows the exponents of ω in (2) to attain any value between 0 and 2, which is not possible using the classical TBBF.

B. PROPOSED TECHNIQUE

The proposed FO-TBBF approximant $G(s)$ is modeled according to (3):

$$G(s) = \begin{cases} \dfrac{k(s^2+z_1 s+z_2)}{\prod_{i=1}^{(n_1+3)/2}(s^2+p_i s+p_i')}, & \text{if } n_1 \text{ is odd;} \\ \dfrac{k(s^2+z_1 s+z_2)}{(s+p_0)\prod_{i=1}^{(n_1+2)/2}(s^2+p_i s+p_i')}, & \text{if } n_1 \text{ is even.} \end{cases} \tag{3}$$

The resulting integer order of the approximant $G(s)$, as defined by (3), is determined as n_1+3. The approximation of the magnitude-frequency response of the normalized FO-TBBF is formulated as an optimization problem by minimizing the cost function f, as proposed in (4):

$$f = \sum_{i=1}^{L} |20\log_{10}|B(j\omega_i)| - 20\log_{10}|G(j\omega_i, X)||^2. \tag{4}$$

Subject to:

$$\begin{cases} z_i > 0, (i = 1, 2); \\ p_i, p_i' > 0, (i = 1, 2, \ldots, \dfrac{n_1+3}{2}) & \text{if } n_1 \text{ is odd;} \\ p_0 > 0; p_i, p_i' > 0, (i = 1, 2, \ldots, \dfrac{n_1+2}{2}) & \text{if } n_1 \text{ is even.} \end{cases}$$

where L denotes the total number of frequency points logarithmically distributed in the interval $\omega \in [\omega_{\min}, \omega_{\max}]$ rad/s; and X represents the vector of decision variables. For odd values of n_1, $X = [k\ z_1\ z_2\ p_1\ p_1'\ p_2\ p_2' \ldots p_{(n_1+3)/2}\ p'_{(n_1+3)/2}]$;

TABLE 2. Optimal design variables vector (X) and the coefficient of determination (R^2) for the proposed FO-TBBFs.

No.	n_1	n_2	α	β	X	R^2
1	0	0	0.8	0.5	3.4577 20.5781 26.3290 3.5561 35.9890 26.1070	0.999202
2	1	0	0.6	0.8	10.7612 40.3285 190.1239 92.0139 922.8042 2.9512 2.2192	0.999988
3	1	1	0.9	0.2	2.2825 35.6773 109.2299 1.8751 1.3225 45.4461 188.1357	0.999980
4	2	0	0.4	0.7	30.9903 30.5457 98.3527 103.7628 13.5594 15.9953 1.9830 1.8489	0.999894
5	2	1	0.5	0.5	18.8685 41.7971 219.0603 14.6302 102.6382 259.3795 1.4536 1.0897	0.999996
6	2	2	0.8	0.1	3.8256 44.7456 220.9040 59.5282 1.2455 1.0200 10.1736 13.9340	0.999991
7	3	0	0.1	0.3	206.5309 14.8654 1.3352 1.1941 1.4929 212.2080 17.8776 12.6353 10.5320	0.999984
8	3	1	0.7	0.6	6.4543 45.9104 251.8496 1.0675 1.1947 2.5708 1.7000 83.8318 799.2386	0.999989
9	3	2	0.5	0.2	19.0275 43.1617 236.5874 1.0347 1.0747 17.7539 38.5183 103.1746 108.6580	0.999995
10	3	3	0.9	0.4	2.3133 47.3617 245.4966 0.8255 0.9885 9.0383 9.9527 52.9365 57.6942	0.999998
11	4	0	0.2	0.4	96.0684 17.5756 8.1852 10.9305 143.7563 49.9895 1.5052 1.0674 0.9659 1.3691	0.999919
12	4	1	0.6	0.3	11.2103 49.1477 314.7206 14.8100 94.3385 240.6904 0.8246 1.2808 1.4934 0.7729	0.999997
13	4	2	0.8	0.9	3.9069 54.3350 369.2132 11.2591 1.7575 1.0689 0.7938 1.0981 70.3600 109.2098	0.999998
14	4	3	0.7	0.7	6.6053 53.0182 365.0728 13.4444 0.7307 1.0320 1.6772 0.9116 83.0111 190.7630	0.999998
15	4	4	0.9	0.1	2.3428 57.3502 398.5279 9.7607 0.6809 1.0133 61.7819 101.3200 1.6865 0.9320	0.999999

if n_1 is even, then $X = [k\ z_1\ z_2\ p_0\ p_1\ p_1'\ p_2\ p_2'\ \cdots p_{(n_1+2)/2}\ p'_{(n_1+2)/2}]$.

The constraints can be satisfied by choosing a positive value for the lower bound of the decision variables. Hence, the proposed optimization problem can be solved using any unconstrained global search optimization technique.

C. ALGORITHM IMPLEMENTATION

Algorithm 1 presents the pseudocode to implement the proposed optimization routine for a single trial run. In order to guarantee the generation of a stable rational approximant, the lower bound (Lb) for all decision variables (except k) is set as 10^{-4}; in the case of k, Lb may be fixed as 0. A large value of upper bound (Ub) needs to be avoided since it may result in a large dispersion of the decision variables. A wide variation in the coefficients of the FO-TBBF transfer function will lead to larger spreading (ranging from a few ohms to several mega-ohms) in the values of passive components, which is undesirable for the practical implementation. To attain the passive components values within practical limits, Ub may be chosen as 1000. The initial point is randomly varied *iter* times between Lb and $(Lb + c)$, where $c \in \mathbb{Z}^+$. A single trial run of the optimization algorithm generates an *iter* number of solutions; the best solution (X_{best}) is the one that attains the smallest value of the error fitness function ($f_{\min}$). Thirty independent trial runs of the algorithm are executed for each design case to identify the most accurate model.

Algorithm 1 The Proposed Algorithm Pseudocode

Inputs : n_1, n_2, α, β
Outputs: $X_{\text{best}}, f_{\min}$

begin
  Set $\omega_{\min}, \omega_{\max}, L, iter, c, Lb, Ub$
  for $i = 1$ **to** *iter* **do**
    X_0 (Initial point of X) $\in rand(Lb, Lb + c)$
    $B(s) \leftarrow ks^2 + kz_1 s + kz_2$
    if ($n_1 == Odd$) **then**
      $A(s) \leftarrow 1$
      for $j = 1$ **to** $(n_1 + 3)/2$ **do**
        $A(s) \leftarrow A(s) \times (s^2 + p_j s + p_j')$
    else
      $A(s) \leftarrow (s + p_0)$
      for $j = 1$ **to** $(n_1 + 2)/2$ **do**
        $A(s) \leftarrow A(s) \times (s^2 + p_j s + p_j')$
    $G(s) \leftarrow B(s)/A(s)$
    Minimize (4) and store f_i
    Store X_i
  $f_{\min} \leftarrow \min\{f_i\}$
  $X_{\text{best}} \leftarrow X_i$ corresponding to $f_{\min}$

III. SIMULATION RESULTS

The MATLAB based optimization routine uses the solver *fmincon* (algorithm: '*active-set*') with the following arguments: $MaxFunEvals = 50000$; $MaxIter = 5000$; $TolFun =$ 1E–10; and $TolX =$ 1E–10. The optimal values of the decision variables for 15 design examples, with $[\omega_{\min}, \omega_{\max}] = [10^{-2}, 10^2]$ rad/s, $\varepsilon^2 = 0.5$, $L = 50$, $iter = 100$, $c = 10$, and $Ub = 1000$, are presented in Table 2. To quantify the effectiveness of the modeling accuracy, the coefficient of determination (R^2) index (evaluated for L magnitude-frequency data sample points) is also shown in Table 2. A higher value of R^2 (in ideal case 1) indicates a better fitting of the proposed model to the theoretical one. Except for no. 1 and 4 [$(n_1, n_2, \alpha, \beta) = (0, 0, 0.8, 0.5)$ and $(2, 0, 0.4, 0.7)$], all other designs achieve $R^2 > 0.9999$, which highlights a good agreement in the magnitude responses of the optimal model with the ideal FO-TBBF. The proposed method can also attain the same solution quality for other values of c, such as 100 and 1000.

Table 3 presents the minimum (min), maximum (max), mean, and standard deviation (SD) indices of $f_{\min}$ for all considered design cases based on 30 runs. Out of the 15 examples, 13 cases yield the same fitness values for min, max, and mean indices. This implies that the same solution quality is obtained irrespective of the number of independent trial runs of the optimization technique. The excellent robustness of the proposed technique is further highlighted by the small value of the SD index.

The magnitude plot of the proposed model for no. 1 [$(n_1, n_2, \alpha, \beta) = (0, 0, 0.8, 0.5)$] attains agreement with the

TABLE 3. Statistical indices to evaluate the average performance of the fitness value based on 30 runs.

No.	n_1	n_2	α	β	min	max	mean	SD
1	0	0	0.8	0.5	1.0377	1.0377	1.0377	2.78E–10
2	1	0	0.6	0.8	0.0758	0.0794	0.0770	1.80E–3
3	1	1	0.9	0.2	0.0559	0.0559	0.0559	2.51E–9
4	2	0	0.4	0.7	0.2139	0.2139	0.2139	1.35E–9
5	2	1	0.5	0.5	0.0450	0.0450	0.0450	1.48E–9
6	2	2	0.8	0.1	0.0427	0.0427	0.0427	2.07E–9
7	3	0	0.1	0.3	0.0719	0.0719	0.0719	1.14E–9
8	3	1	0.7	0.6	0.0478	0.0492	0.0483	6.51E–4
9	3	2	0.5	0.2	0.0399	0.0399	0.0399	1.74E–9
10	3	3	0.9	0.4	0.0132	0.0132	0.0132	3.34E–9
11	4	0	0.2	0.4	0.2285	0.2285	0.2285	2.16E–9
12	4	1	0.6	0.3	0.0246	0.0246	0.0246	2.90E–9
13	4	2	0.8	0.9	0.0140	0.0140	0.0140	6.44E–9
14	4	3	0.7	0.7	0.0184	0.0184	0.0184	4.50E–9
15	4	4	0.9	0.1	0.0046	0.0046	0.0046	1.61E–8

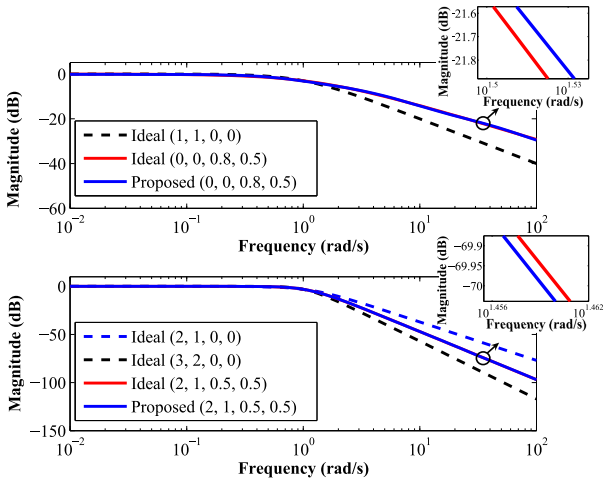

FIGURE 1. MATLAB-simulated magnitude-frequency response comparison plots of the proposed FO-TBBFs. Note that the numbers within the parenthesis represent $(n_1, n_2, \alpha, \beta)$.

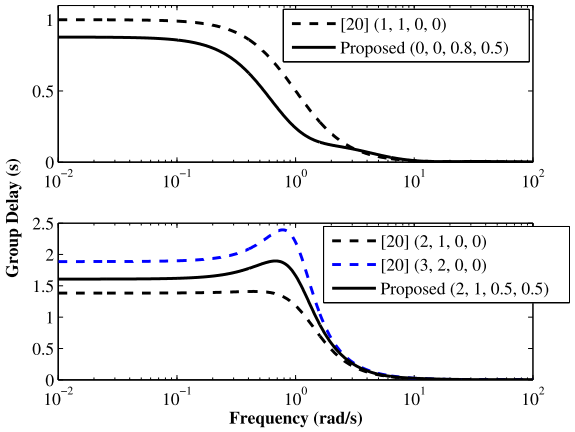

FIGURE 2. MATLAB-simulated group delay plots of the proposed FO-TBBFs as compared with the classical TBBFs reported in [20]. Note that the numbers within the parenthesis represent $(n_1, n_2, \alpha, \beta)$.

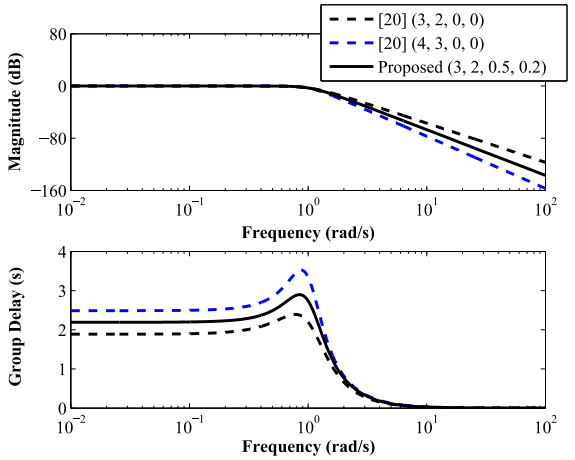

FIGURE 3. Comparisons of MATLAB-simulated magnitude and group delay plots of the proposed FO-TBBF with the classical TBBFs reported in [20]. Note that the numbers within the parenthesis represent $(n_1, n_2, \alpha, \beta)$.

theoretical behavior, as shown in Figure 1 (top). This figure also demonstrates that the roll-off characteristics for the FO-TBBF can extend below the one obtained for the lowest order of the classical TBBF ($n = k = 1$). As another test case, Figure 1 (bottom) shows the magnitude response for the proposed design no. 5 $[(n_1, n_2, \alpha, \beta) = (2, 1, 0.5, 0.5)]$. A close match with the ideal characteristics ($R^2 = 0.999996$) may be noted. The fractional stepping for the proposed FO-TBBF is highlighted in the same figure by presenting the magnitude plots of the TBBFs for $(n = 2, k = 1)$ and $(n = 3, k = 2)$.

Figure 2 (top) illustrates the smaller group delay of the proposed model no. 1 compared to the classical TBBF ($n = k = 1$) reported in [20]. Group delay comparisons of the proposed approximant for no. 5 with the classical TBBFs cited in [20] for $(n = 2, k = 1)$ and $(n = 3, k = 2)$ are shown in Figure 2 (bottom). Results reveal that the group delay behavior of the optimal model lies in-between the responses of the classical filters.

To further highlight the FO modeling behavior of the proposed designs, the magnitude (top) and group delay (bottom) plots of the FO-TBBF for model no. 9 $[(n_1, n_2, \alpha, \beta) =$ $(3, 2, 0.5, 0.2)]$ are compared with the classical TBBFs [20] for $(n = 3, k = 2)$ and $(n = 4, k = 3)$, as shown in Figure 3. Both these plots confirm that the proposed FO-TBBF can achieve the frequency responses which may not be yielded using the classical TBBFs.

The effectiveness of the proposed models in attaining a smaller group delay in the passband as compared to the FOBF is also demonstrated. For this purpose, the magnitude (top) and group delay (bottom) responses of the 1.6^{th}-order FOBF reported in [22] are compared with the proposed FO-TBBF model no. 2 $[(n_1, n_2, \alpha, \beta) = (1, 0, 0.6, 0.8)]$, as presented in Figure 4. It may be noted that since the stopband attenuation characteristic for the FO-TBBF is dominated by the $(n_1 + \alpha)^{\text{th}}$-order Butterworth filter, hence, the magnitude roll-off rate for the proposed FO-TBBF is similar to that of the FOBF of order 1.6. The magnitudes of the FO-TBBF at the frequencies of 10 rad/s and 100 rad/s are -29.06 dB and -61.08 dB, respectively. Therefore, the roll-off rate for the FO-TBBF is -32.02 decibel/decade (dB/dec), which is close to the theoretical value of -32.0 dB/dec obtained for

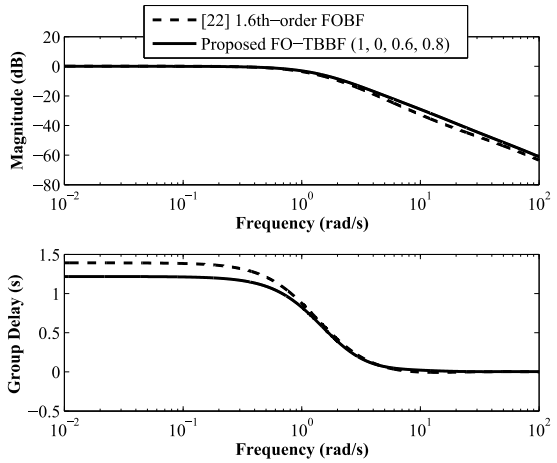

FIGURE 4. **Comparisons of MATLAB-simulated magnitude and group delay plots of the proposed FO-TBBF with the FOBF reported in [22]. Note that the numbers within the parenthesis represent (n_1, n_2, α, β).**

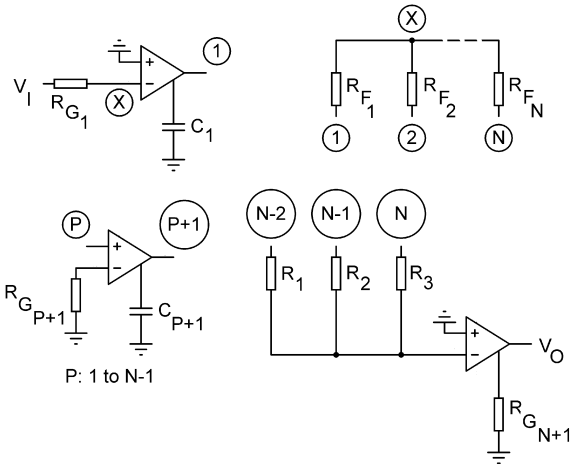

FIGURE 5. **CFOA-based circuit implementation of the proposed FO-TBBF approximant.**

the 1.6$^{\text{th}}$-order FOBF. However, the maximum group delay achieved for the proposed FO-TBBF (1.217 s) is substantially smaller as compared to the reported FOBF model [22] (1.392 s). This is due to the fact that the dominating response in the passband for the FO-TBBF depends on the $(n_2 + \beta)^{\text{th}}$-order Butterworth filter, which is of order 0.8 in the present case. Thus, the proposed design achieves an improved group delay performance as compared to the FOBF without compromising the stopband behavior.

IV. CIRCUIT IMPLEMENTATION AND EXPERIMENTAL VERIFICATION

The circuit realization of the FO-TBBF approximants is demonstrated using the CFOA employed in a follow-the-leader feedback topology [24]. The complete circuit can be constructed using the nodal connections shown in Figure 5. For e.g., nodes P and X are respectively represented as Ⓟ and Ⓧ in the figure. Source input and signal output voltages of the circuit are denoted by V_{I} and V_{O}, respectively. The series connections of the CFOAs between the nodes Ⓟ and Ⓟ+1 are carried out for P varying from 1 to $N-1$, where $N = n_1 + 3$. The total number of amplifiers, resistors, and capacitors needed to realize the FO-TBBF model are $N+1$, $2N+4$, and N, respectively. Thus, $3N+4$ number of design variables is required to realize the circuit. The transfer function of the proposed circuit is given by (5):

$$\frac{V_{\text{O}}(s)}{V_{\text{I}}(s)} = \frac{\displaystyle\sum_{k=0}^{2} \frac{R_{\text{G}_{N+1}} s^k}{R_{3-k} \displaystyle\prod_{i=1}^{N-k} C_i R_{\text{G}_i}}}{s^N + \dfrac{s^{N-1}}{R_{\text{F}_1} C_1} + \displaystyle\sum_{k=0}^{N-2} \frac{s^k}{C_1 R_{\text{F}_{N-k}} \displaystyle\prod_{i=2}^{N-k} C_i R_{\text{G}_i}}}. \quad (5)$$

The values of the R-C components are determined by comparing (3) and (5), which results in $(N+3)$ independent equations. Hence, the values for $(2N+1)$ number of passive components can be initially chosen. As a representative, the circuit realization steps of the proposed FO-TBBF model no. 5 for $(n_1, n_2, \alpha, \beta) = (2, 1, 0.5, 0.5)$ are presented as follows:

(i) Set $n_1 = 2$. Therefore, $N = 5$. The circuit comprises 6 CFOAs, 14 resistors, and 5 capacitors. The value of P is incremented from 1 to 4,

(ii) Set the desired cut-off frequency of the filter, such as $f_{\text{c}} = 1$ kHz,

(iii) Eight modeling equations relate the circuit transfer function to the coefficients of $G(s)$. The number of design variables is 19. Therefore, the values of 11 passive elements are initially set,

(iv) The passive components are selected from the E-24 standard industrial series for the resistors and the E-12 series for the capacitors. The following resistor values are set as: $R_{\text{F}_1} = R_{\text{F}_2} = R_{\text{F}_3} = R_{\text{F}_4} = R_{\text{F}_5} = 10$ kΩ, $R_{\text{G}_1} = 100$ kΩ, $R_{\text{G}_2} = 1$ kΩ, $R_{\text{G}_3} = R_{\text{G}_4} = R_{\text{G}_5} = 10$ kΩ, and $R_1 = 270$ kΩ. The values of the other R-C components are derived as follows: $R_{\text{G}_6} = 8.2$ kΩ, $C_1 = 0.12$ nF, $C_2 = 10$ nF, $C_3 = 4.7$ nF, $C_4 = 15$ nF, $C_5 = 27$ nF, $R_2 = 7.5$ kΩ, and $R_3 = 750$ Ω.

The circuit for the proposed FO-TBBF no. 5 was assembled on a breadboard using the above listed R-C component values. The supply voltage for Analog Devices AD844AN amplifiers was provided by the Agilent E3630A power supply. The frequency responses of the FO-TBBF were measured by the OMICRON Lab Bode 100 network analyzer. 401 logarithmically spaced frequency points in the range 10 Hz to 100 kHz were considered. The level of the testing harmonic signal was set to 10 dBm (0.7071 V_{RMS}). The receiver bandwidth of the analyzer was fixed at 10 Hz to obtain precise results. The THRU calibration of the analyzer was performed before the measurement to eliminate the influence of the measurement setup. After connecting the proposed FO-TBBF circuit to the analyzer, the frequency responses were measured and displayed by the connected computer with the Bode Analyzer Suite software. The photograph of the hardware setup is presented in Figure 6.

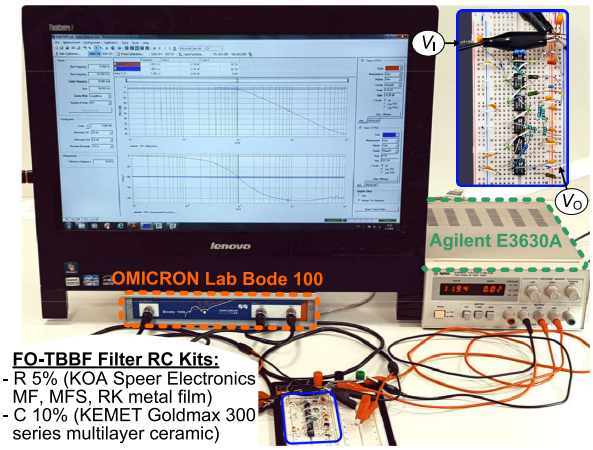

FIGURE 6. Photo of the experimental set-up.

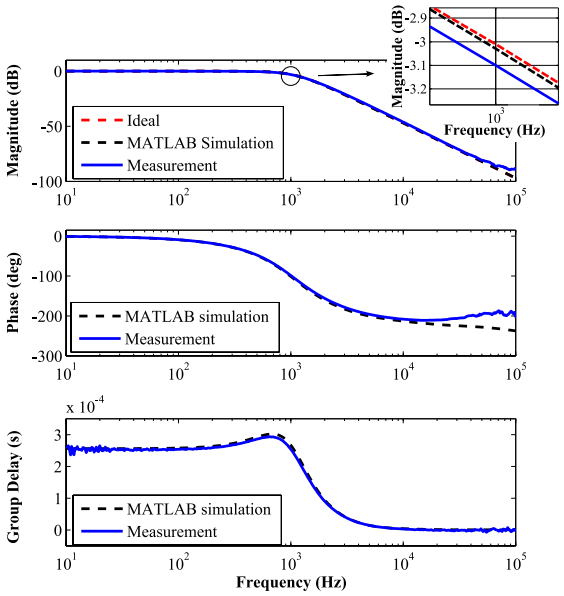

FIGURE 7. Magnitude, phase, and group delay vs. frequency plots of the proposed FO-TBBF for $(n_1, n_2, \alpha, \beta) = (2, 1, 0.5, 0.5)$.

The magnitude-frequency response measurements of the proposed FO-TBBF are compared with the ideal and simulated ones in Figure 7 (top). The practical filter demonstrates excellent agreement with the ideal characteristic up to nearly 70 kHz. The magnitude of the approximant at $f_c = 1$ kHz for measurement (–3.100 dB) demonstrates conformity with the ideal (–3.010 dB) and MATLAB simulations (–3.029 dB). R^2 of 0.999968 is achieved for the measured magnitude response data compared to the theoretical one. Figure 7 also depicts the experimental results for the phase (middle) and group delay frequency responses (bottom) of the FO-TBBF. Comparisons with the simulated plots highlight excellent matching of the phase plot for nearly 3 decades and the group delay for the entire design bandwidth.

V. CONCLUSION

Optimal and robust modeling of several frequency characteristics for the FO-TBBF is introduced. The generalization of the classical TBBF results in more precise control of the magnitude, phase, and group delay behaviors. The efficient modeling performance of the proposed technique is validated through numerical simulations and experiments made on CFOA-based circuit implementation.

REFERENCES

[1] P. Mitros, "Filters with decreased passband error," *IEEE Trans. Circuits Syst. II, Exp. Briefs*, vol. 63, no. 2, pp. 131–135, Feb. 2016, doi: 10.1109/TCSII.2015.2483377.
[2] H. G. Dimopoulos, "Optimal use of some classical approximations in filter design," *IEEE Trans. Circuits Syst. II, Exp. Briefs*, vol. 54, no. 9, pp. 780–784, Sep. 2007, doi: 10.1109/TCSII.2007.900345.
[3] N. T. Hoang, H. D. Tuan, T. Q. Nguyen, and H. G. Hoang, "Optimized analog filter designs with flat responses by semidefinite programming," *IEEE Trans. Signal Process.*, vol. 57, no. 3, pp. 944–955, Mar. 2009, doi: 10.1109/TSP.2008.2009021.
[4] H. G. Hoang, H. D. Tuan, and T. Q. Nguyen, "Optimized analog flat filter design," *IEEE Trans. Signal Process.*, vol. 58, no. 2, pp. 901–906, Feb. 2010, doi: 10.1109/TSP.2009.2028956.
[5] A. S. Elwakil, "Fractional-order circuits and systems: An emerging interdisciplinary research area," *IEEE Circuits Syst. Mag.*, vol. 10, no. 4, pp. 40–50, Nov. 2010, doi: 10.1109/MCAS.2010.938637.
[6] D. A. John, S. Banerjee, and K. Biswas, "Nanocomposite material characterization of a solid-state fractional capacitor," *IEEE Trans. Electron Devices*, vol. 67, no. 3, pp. 1136–1142, Mar. 2020, doi: 10.1109/TED.2020.2965432.
[7] G. Tsirimokou, C. Psychalinos, A. S. Elwakil, and K. N. Salama, "Electronically tunable fully integrated fractional-order resonator," *IEEE Trans. Circuits Syst. II, Exp. Briefs*, vol. 65, no. 2, pp. 166–170, Feb. 2018, doi: 10.1109/TCSII.2017.2684710.
[8] A. Adhikary, S. Choudhary, and S. Sen, "Optimal design for realizing a grounded fractional order inductor using GIC," *IEEE Trans. Circuits Syst. I, Reg. Papers*, vol. 65, no. 8, pp. 2411–2421, Aug. 2018, doi: 10.1109/TCSI.2017.2787464.
[9] A. S. Ali, A. G. Radwan, and A. M. Soliman, "Fractional order Butterworth filter: Active and passive realizations," *IEEE J. Emerg. Sel. Topics Circuits Syst.*, vol. 3, no. 3, pp. 346–354, Sep. 2013, doi: 10.1109/JETCAS.2013.2266753.
[10] A. G. Radwan, A. S. Elwakil, and A. M. Soliman, "Fractional-order sinusoidal oscillators: Design procedure and practical examples," *IEEE Trans. Circuits Syst. I, Reg. Papers*, vol. 55, no. 7, pp. 2051–2063, Aug. 2008, doi: 10.1109/TCSI.2008.918196.
[11] A. Adhikary, S. Sen, and K. Biswas, "Practical realization of tunable fractional order parallel resonator and fractional order filters," *IEEE Trans. Circuits Syst. I, Reg. Papers*, vol. 63, no. 8, pp. 1142–1151, Aug. 2016, doi: 10.1109/TCSI.2016.2568262.
[12] A. G. Radwan and K. N. Salama, "Passive and active elements using fractional $L_\beta C_\alpha$ circuit," *IEEE Trans. Circuits Syst. I, Reg. Papers*, vol. 58, no. 10, pp. 2388–2397, Oct. 2011, doi: 10.1109/TCSI.2011.2142690.
[13] M. S. Sarafraz and M. S. Tavazoei, "Realizability of fractional-order impedances by passive electrical networks composed of a fractional capacitor and RLC components," *IEEE Trans. Circuits Syst. I, Reg. Papers*, vol. 62, no. 12, pp. 2829–2835, Dec. 2015, doi: 10.1109/TCSI.2015.2482340.
[14] H. Nezzari, A. Charef, and D. Boucherma, "Analog circuit implementation of fractional order damped sine and cosine functions," *IEEE J. Emerging Sel. Topics Circuits Syst.*, vol. 3, no. 3, pp. 386–393, Sep. 2013, doi: 10.1109/JETCAS.2013.2273854.
[15] A. Oustaloup, F. Levron, B. Mathieu, and F. M. Nanot, "Frequency-band complex noninteger differentiator: Characterization and synthesis," *IEEE Trans. Circuits Syst. I, Fundam. Theory Appl.*, vol. 47, no. 1, pp. 25–39, Jan. 2000, doi: 10.1109/81.817385.
[16] A. M. AbdelAty, A. S. Elwakil, A. G. Radwan, C. Psychalinos, and B. J. Maundy, "Approximation of the fractional-order Laplacian s^α as a weighted sum of first-order high-pass filters," *IEEE Trans. Circuits Syst. II, Exp. Briefs*, vol. 65, no. 8, pp. 1114–1118, Aug. 2018., doi: 10.1109/TCSII.2018.2808949.
[17] A. Budak and P. Aronhime, "Transitional butterworth-chebyshev filters," *IEEE Trans. Circuit Theory*, vol. IT-18, no. 3, pp. 413–415, May 1971, doi: 10.1109/TCT.1971.1083276.
[18] G. Aiello and P. Angelo, "Transitional Legendre Thomson filters," *IEEE Trans. Circuits Syst.*, vol. CAS-21, no. 1, pp. 159–162, Jan. 1974, doi: 10.1109/TCS.1974.1083782.

[19] J. R. Johnson, D. E. Johnson, and R. J. Lacarna, "TUT and TABU transitional filters," *J. Franklin Inst.*, vol. 307, no. 3, pp. 175–182, 1979, doi: 10.1016/0016-0032(79)90016-4.
[20] C. S. Lindquist and C. A. Corral, "A new type of transitional filter based on summation of polynomials," *J. Franklin Inst.*, vol. 342, no. 5, pp. 447–472, Aug. 2005, doi: 10.1016/j.jfranklin.2005.01.003.
[21] S. Mahata, S. K. Saha, R. Kar, and D. Mandal, "Approximation of fractional-order low-pass filter," *IET Signal Process.*, vol. 13, no. 1, pp. 112–124, Feb. 2019, doi: 10.1049/iet-spr.2018.5128.
[22] S. Mahata, N. Herencsar, and D. Kubanek, "Optimal approximation of fractional-order Butterworth filter based on weighted sum of classical Butterworth filters," *IEEE Access*, vol. 9, pp. 81097–81114, 2021, doi: 10.1109/ACCESS.2021.3085515.
[23] R. Senani, D. R. Bhaskar, A. K. Singh, and V. K. Singh, *Current Feedback Operational Amplifiers and Their Applications*. New York, NY, USA: Springer, 2013, p. 249.
[24] K. Laker, R. Schaumann, and M. Ghausi, "Multiple-loop feedback topologies for the design of low-sensitivity active filters (invited paper)," *IEEE Trans. Circuits Syst.*, vol. CAS-26, no. 1, pp. 1–21, Jan. 1979, doi: 10.1109/TCS.1979.1084554.

SHIBENDU MAHATA received the M.Tech. degree in instrumentation and electronics engineering from Jadavpur University, India, in 2010. He was a Field Operations and Panel Engineer with Reliance Industries Ltd., and a Research Assistant with the Department of Cybernetics, CSIR-CMERI. He has authored above 40 articles published in SCI-E peer-reviewed journals, conference proceedings, and book chapters. His research interests include optimal modeling of fractional-order analog and digital filters. He was awarded with the University Medal for his M.Tech. degree from Jadavpur University. He was a recipient of the 2019 Premium Award for Best Paper from *IET Signal Processing*.

NORBERT HERENCSAR (Senior Member, IEEE) received the Ph.D. degree from Brno University of Technology (BUT), Czech Republic, in 2010. From 2013 to 2014, he was a Visiting Researcher with Boğaziçi University, Turkey, and Doğuş University, Turkey, for five months. In 2019, he was a Visiting Professor with the University of Calgary, Canada, for six months. Since 2015, he has been an Associate Professor with the Department of Telecommunications, BUT. Since 2006, he has been collaborating on numerous research projects supported by Czech Science Foundation. From 2016 to 2021, he was the Science Communications Manager and an MC Member of the COST Action CA15225 "Fractional-Order Systems-Analysis, Synthesis and Their Importance for Future Design." He has authored 104 articles published in SCI-E peer-reviewed journals and 122 papers in conference proceedings. His research interests include analog electronics, bioimpedance modeling, energy storage elements, fractional-order circuits and systems, impedance spectroscopy, instrumentation and measurement, sensory processing circuits and systems, and VLSI analog integrated circuits. Since 2013, he has been an Organizing or a TPC Member of AFRICON, ELECO, I^2MTC, ICUMT, IWSSIP, SETCAS, MWSCAS, and ICECS conferences. He is a Senior Member of IACSIT and IRED, and a member of IAENG, ACEEE, and RS. From 2008 to 2016 and from 2017 to 2020, he was an Organizing Committee Member and the General Co-Chair of the International Conference on Telecommunications and Signal Processing (TSP). Since 2015, he has been serving for the IEEE Czechoslovakia Section Executive Committee as an SP/CAS/COM Joint Chapter Chair. Since 2021, he has been the General Chair of TSP. Since 2011, he has been contributing as a Guest Co-Editor to several special journal issues in *AEÜ—International Journal of Electronics and Communications*, *Applied Sciences*, *Radioengineering*, *Telecommunication Systems*, and *Sensors*. Since 2014, he has been serving as an Associate Editor for IEEE Access, *IEICE Electronics Express* (ELEX), and *Journal of Circuits, Systems and Computers*; an Editorial Board Member for the *Elektronika ir Elektrotechnika* and *Radioengineering*; and a Topics Board Member for the *Nanomaterials*. In July 2021, he was appointed as the Editor-in-Chief of the Engineering Section of *Fractal and Fractional*. He is ranked among World's Top 2% Scientists reported by Stanford University.

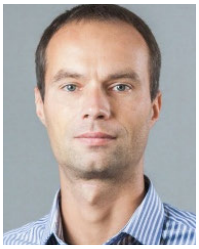

DAVID KUBANEK received the M.S. degree in electronics and communication and the Ph.D. degree in teleinformatics from Brno University of Technology (BUT), Czech Republic, in 2002 and 2006, respectively. Since 2006, he has been an Assistant Professor with the Department of Telecommunications, BUT. He has authored 24 articles published in SCI-E peer-reviewed journals and about 35 papers in conference proceedings. He has participated on numerous research projects supported by Czech Science Foundation. His research interests include design and analysis of analog electronic circuits, devices and elements, frequency filters, oscillators, impedance converters, non-linear circuits, and fractional-order circuits and systems. Since 2019, he has been serving as an Editorial Board Member for *Fractal and Fractional* journal.

RAJIB KAR (Senior Member, IEEE) received the B.E. degree in electronics and communication engineering from Regional Engineering College, Durgapur, West Bengal, India, in 2001, and the M.Tech. and Ph.D. degrees from the National Institute of Technology, Durgapur, West Bengal, India, in 2008 and 2011, respectively. He is currently attached with the National Institute of Technology, Durgapur, as an Associate Professor with the Department of Electronics and Communication Engineering. He has published more than 130 research articles in international journals. He has guided ten Ph.D. students in his domain of research. His research interests include VLSI circuit optimization and signal processing via evolutionary computing techniques. He was awarded Visvesaraya YFRF by Meity, GOI, in 2016.

DURBADAL MANDAL (Member, IEEE) received the B.E., M.Tech., and Ph.D. degrees from the National Institute of Technology, Durgapur, West Bengal, India. He is currently attached with the National Institute of Technology, Durgapur, as an Associate Professor with the Department of Electronics and Communication Engineering. He has published more than 300 research papers in international journals and conferences. He has produced 13 Ph.D. students to date. His research interests include array antenna design and digital filter optimization via evolutionary optimization techniques.

İ. CEM GÖKNAR (Life Fellow, IEEE) was born in Istanbul, Turkey. He received the B.Sc. and M.Sc. degrees from Istanbul Technical University and the Ph.D. degree from Michigan State University, in 1969. He was a Visiting Professor at the University of California at Berkeley, the University of Illinois at Urbana-Champaign, the University of Waterloo, ON, Canada, and Technical University of Denmark, Lyngby. He gave lectures at the University of Sannio, Italy; the University of Pavia, Italy; the University of Lisbon, Portugal; and Brno University of Technology, Czech Republic. He was the Director of the Science and Technology Institute, Işik University, where he is currently a Professor. He has been on the European Circuit Society Council, in 1995, which he chaired from 2009 to 2011. He received NATO's Senior Scientist Grant (1974) and Minna-James-Heineman-Stiftung Award (1980). He was the IEEE-CAS Chapter Chair, Turkey, which received the IEEE CAS-Tr Chapter of the Year Award, in 2014.